Glass tempering heat transfer coefficient evaluation and air jets parameter optimization

F. Cirillo, G.M. Isopi

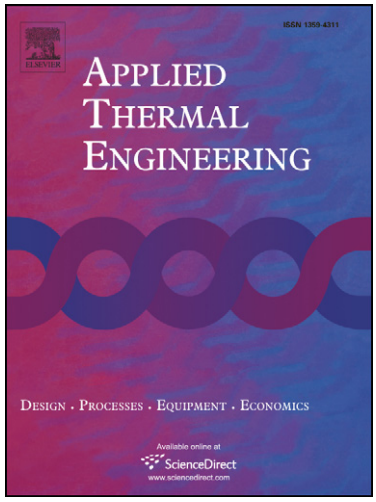

Glass tempering heat transfer coefficient evaluation and air jets parameter optimization

F. Cirillo, G.M. Isopi

PII: S1359-4311(08)00270-6
DOI: 10.1016/j.applthermaleng.2008.06.005
Reference: ATE 2540

To appear in: *Applied Thermal Engineering*

Received Date: 10 July 2006
Revised Date: 2 October 2007
Accepted Date: 8 June 2008

Please cite this article as: F. Cirillo, G.M. Isopi, Glass tempering heat transfer coefficient evaluation and air jets parameter optimization, *Applied Thermal Engineering* (2008), doi: 10.1016/j.applthermaleng.2008.06.005

Glass tempering heat transfer coefficient evaluation and air jets parameter optimization

F. Cirillo [1], G.M. Isopi *

Dipartimento di Meccanica e Aeronautica, Universitá degli studi di Roma "La Sapienza", Via Eudossiana 18, 00184 Roma, Italia

Abstract

A Design OF Experiments (DOE) matrix of CFD simulations is used to create a mathematical model able to calculate the heat transfer coefficient for nine circular confined air jets vertically impinging on a flat plate. Typical air jets dimensions and process parameter values used in glass tempering are evaluated. The flat plate temperature is set to the constant value of $640°C$. Two different values of jet diameter (4mm, 8mm), of air velocity at nozzle exit (110m/s, 140m/s), of jet-to-jet spacing (40mm, 60mm), of jet-to-plate distance (40mm, 60mm) and of nozzle height (20mm, 60mm) are considered. Implemented into a Visual Basic application, the mathematical model found allow the instant evaluation of heat transfer parameters and to optimize air jets parameter configuration.

Key words: Computational Fluid Dynamics, Design Of Experiments, Glass tempering, Impinging jet, Heat transfer.

1 Introduction

Many industrial activities make use of air jets impingement process: tempering and shaping of glass; cooling of electronic devices and gas turbine blades; paper and textiles drying. The importance of these activities has led many researchers to better understand heat transfer phenomena caused by air jets impinging on hot or cold surfaces; thus, a lot of experimental work has been

* Corresponding author. Tel.: +39 065812722
Email addresses: f.cirillo@dma.ing.uniroma1.it (F. Cirillo), giovanni.isopi@uniroma1.it (G.M. Isopi).
[1] Tel.:+39 0644585243 - 065812722

done since a solution of this intrinsic complex phenomenon can not rely on analytical methods.

Nomenclature

Latin letters

CFD	Computational Fluid Dynamics	
DOE	Design Of Experiments	
DOF	Degree Of Freedom	
D	Nozzle exit diameter	mm
H	Jet-to-plate distance	mm
h	Average heat transfer coefficient	$J/(m^2 \cdot s \cdot^\circ C)$
MS	Mean Square due to a control factor	
Re	Reynolds number	VD/ν
S	Jet-to-jet spacing	mm
Se^2	Mean Square due to experimental error	
Sp	Nozzle height	mm
U	Uniformity parameter	
V	Air velocity at nozzle exit	m/s

Greek letters

ν	Kinematic viscosity	m^2/s

This complexity is well described by Jung-Yang San and Mao-De Lai(1). Depending on the values of $S/D, H/D$ and Reynolds number, two main flow configurations can occur. For small values of S/D - relative to H/D and Re - the interaction between adjacent jets, before impingement, will weaken the jets strength, thus reducing the heat transfer coefficient value (Fig. 1(a)). With S/D increasing the interaction between adjacent core jets will disappear and, if the Reynolds number is high enough, the interference between adjacent wall jets will generate a recirculation (fountain effect) that will modify the air jets core temperature and thus the heat transfer coefficient (Fig.1(b)). The heat transfer for a single round nozzle and for an array of round nozzles impinging a flat plate was studied by Martin (2). The experimental results of his work is represented by two equations that allow prediction of the average Nusselt

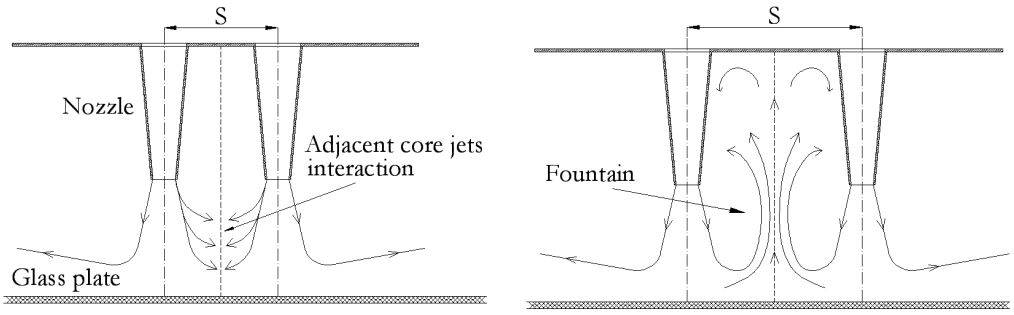

(a) Adjacent core jet interaction. (b) Fountain effect.

Fig. 1. Small values of S/D - relative to H/D and Re - cause the interaction between adjacent core jets, thus reducing the heat transfer coefficient value (fig.1(a)). With S/D increasing and for high values of Reynolds number, the interference between adjacent wall jets can generate a recirculation (fountain effect, fig.1(b)) that will further reduce the heat transfer coefficient.

number for a range of air jet parameter values. Jung-Yang San and Chin-Hao Huang (3) supply an experimental equation to calculate the local Nusselt number for a single round air jet impinging a flat plate, while Huber and Viskanta (4) have examined the influence of spent air exits located between the jets on the value of the local heat transfer coefficient, for a confined square array of 9 round jets impinging a flat heated surface. The same authors investigated the influence of jet-to-jet spacing on the heat transfer coefficient (5) and make a comparison of perimeter and center jets in an array of axisymmetric air jets (6). The effect of effusion holes for air spent discharging, in an array of circular air jets impinging a flat plate, was also studied by Rhee, Yoon and Cho (7). Their results show that the presence of spent air exits is an important factor affecting the dependence of the average heat transfer coefficient value on the gap distance H/D. Moreover, effusion holes allow a more uniform cooling of the impinged surface and increase the average heat transfer coefficient as small values of the jet to plate distance are used.

Another simple equation, which correlate the stagnation Nusselt number with Re number and H/D for a confined circular air jet impinging on a flat plate, is supplied by Jung-Yang San and Wen-Zheng Shiao (8). They performed a series of experiments investigating the influence of the jet to plate distance H/D and plate dimensions on the stagnation Nusselt number. A numerical and experimental investigation of the effect of Re number and gap distance H/D on the flow characteristics of a confined circular air jet impinging a flat surface was carried out by Baydar and Ozmen (9). The results of their numerical study - performed using a standard $\kappa - \epsilon$ turbulence model - show a good agreement with experimental results, for $H/D \geq 1$ and Reynolds numbers ranging from 30,000 to 50,000. The effect of nozzle geometry was studied by Colucci and Viskanta (10), who compared results for two hyperbolic nozzles with those obtained with a confined orifice, and by Dano et. al. (11), who studied two nozzle geometries: circular and cusped ellipse. The effect of an

obliquely impinging circular air jet - relevant for tempering of bended glass - has been studied by Yan and Saniei (12). Finally, Gardon (13; 14; 15) supply an equation to calculate the average heat transfer coefficient for any amount of air jets impinging a flat plate.
Using the equations supplied by Martin and Gardon it would be possible to predict the average heat transfer coefficient depending on values of air jet parameters. However, the experimental correlations of Martin may not be used if the jets emanate from sharp-edged orifices (this is the case of blowers used for glass tempering) instead of bell-shaped nozzles, and both correlations (Martin and Gardon) are not useful in evaluating the uniformity of the cooling process - crucial for the Quality of the tempered glass - for which it is necessary to calculate the values of the local heat transfer coefficient, for the same conditions. Furthermore, the information about the local and average heat transfer coefficients, supplied in the papers reviewed, are valid for experimental parameter values dissimilar to that considered in the glass tempering process.The only authors that supply information at Re number closer to that considered in the present work are Goodro et al. (16). In their work they investigate the effect of Re number (up to 60,000) and Mach number separately, holding one of these parameter constant as the other one is varied.
The present work deals with the evaluation of the average heat transfer coefficient and of the cooling process uniformity (quality parameters) for design parameter values typically used in glass tempering. The main target of this work is to create a mathematical model able to predict the two quality parameters for design input values in the following range:

$4mm \leq D \leq 8mm$
$40mm \leq H \leq 60mm$
$40mm \leq S \leq 60mm$
$110m/s \leq V \leq 140m/s$
$20mm \leq Sp \leq 60mm$

With non-dimensional parameters:
$5 \leq H/D \leq 15$
$5 \leq S/D \leq 15$
$27700 \leq Re \leq 70500$

A description of the design parameters is summarized in Fig.2.

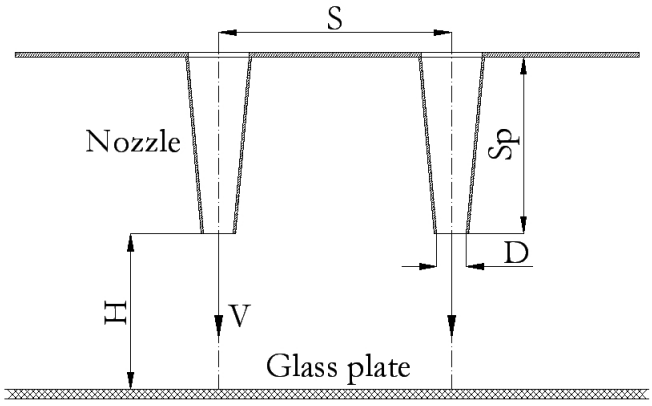

Fig. 2. Design parameters: D (jet diameter), V (air velocity at nozzle exit), S (jet-to-jet spacing), H (jet-to-plate distance) and Sp (nozzle height).

2 DOE Matrix and CFD Model

The DOE approach is useful in every scientific field where an experimental study has to be performed and results evaluated using a limited number of experimental configurations (17). The DOE methodology makes use of matrixes to design a cost-effective set of experiments in order to easily evaluate the influence of each design parameter on a system/process performance, thus dealing to a design optimization, which is the main target in engineering problems (18; 19; 20; 21).
The two quality parameters described in the previous section are the analysis "Target Function" that have to be calculated and used to create the mathematical model. The nozzle exit diameter D, the nozzle-to-plate distance H, the jet-to-jet spacing S, the air velocity at nozzle exit V and nozzle height Sp are two-level "Control Parameters". The Degree Of Freedom (DOF) of each control parameter is equal to:

$$DOF_f = \sharp levels - 1 = 1$$

Thus, an experimental array with at least six rows (experiments) would be necessary to solve the problem(17; 23):

$$\sharp rows(experiments) = (\sharp Control\ Parameters)(DOF_f) + 1$$

Degrees of Freedom is a concept that is useful to describe how big an experiment must be and how much information can be extracted from the experiment(23). The number of unknowns of an experimental setting is equal to the total degrees of freedom for the control parameter (DOF_f, in our case: 5), while the number of equations available is equal to the degrees of freedom

Test	A	B	C	D	E	F	G	H	I	L	M	N	O	P	Q
1	1	1	1	1	1	1	1	1	1	1	1	1	1	1	1
2	1	1	1	1	1	1	1	2	2	2	2	2	2	2	2
3	1	1	1	2	2	2	2	1	1	1	1	2	2	2	2
4	1	1	1	2	2	2	2	2	2	2	2	1	1	1	1
5	1	2	2	1	1	2	2	1	1	2	2	1	1	2	2
6	1	2	2	1	1	2	2	2	2	1	1	2	2	1	1
7	1	2	2	2	2	1	1	1	1	2	2	2	2	1	1
8	1	2	2	2	2	1	1	2	2	1	1	1	1	2	2
9	2	1	2	1	2	1	2	1	2	1	2	1	2	1	2
10	2	1	2	1	2	1	2	2	1	2	1	2	1	2	1
11	2	1	2	2	1	2	1	1	2	1	2	2	1	2	1
12	2	1	2	2	1	2	1	2	1	2	1	1	2	1	2
13	2	2	1	1	2	2	1	1	2	2	1	1	2	2	1
14	2	2	1	1	2	2	1	2	1	1	2	2	1	1	2
15	2	2	1	2	1	1	2	1	2	2	1	2	1	1	2
16	2	2	1	2	1	1	2	2	1	1	2	1	2	2	1

Fig. 3. L16 Orthogonal Matrix. The columns A, B, D, H and Q are assigned to the design parameters (i.e. the Control Parameters) D, H, S, Sp and V respectively. The other columns are used for the interaction analysis.

of a matrix experiment (DOF_{exp}):

$$DOF_{exp} = \sharp rows - 1$$

We are able to solve the problem only if:

$$DOF_f \leq DOF_{exp}$$

thus:

$$\sharp rows \geq 6$$

The interaction (or interference) between D, H, S and V is qualitatively well known(1). Not the same can be said about the interaction between Sp and the other four parameters. With the aim to quantitatively investigate the interference phenomenon occurring between the control parameters, a sixteen experiments matrix is required, since the interference degree of freedom (DOF_{int}) is equal to 10:

$$\sharp rows = DOF_f + DOF_{int} + 1$$

The L16 Orthogonal Matrix(22) suites perfectly the problem (Fig.3),where the columns A, B, D, H and Q are used for the control parameters and the other columns for the two-way interference evaluation. The sixteen-test setting is shown in Table 1.

A 1/8 finite volume model of a configuration with nine circular jets has been developed for each test setting of the orthogonal array, considering the symmetrical behavior of the physical phenomenon (Fig.4).The model radius is set to double the jet-to-jet distance ($2S$).

Table 1
Test setting of the sixteen CFD simulations.

Test n.	D	H	S	Sp	V
1	4	40	40	20	110
2	4	40	40	60	140
3	4	40	60	20	140
4	4	40	60	60	110
5	4	60	40	20	140
6	4	60	40	60	110
7	4	60	60	20	110
8	4	60	60	60	140
9	8	40	40	20	140
10	8	40	40	60	110
11	8	40	60	20	110
12	8	40	60	60	140
13	8	60	40	20	110
14	8	60	40	60	140
15	8	60	60	20	140
16	8	60	60	60	110

In Fig. 5 the models used for test 2 and 12 are shown as an example. The mesh has been automatically generated by the CFD software once the element dimensions are imposed on the model surface. These values were optimized in a previous sensitivity analysis performed on two-dimensional models.
The glass plate temperature is set to the constant value of $640°C$.

3 Results

In Fig. 6 the local heat transfer coefficient values on the glass plate for tests 2 and 12 are shown as a qualitative example. A different scale for the h values has been used ($600\ J/(m^2 \cdot s \cdot^\circ C)$ for test 2 and $1000\ J/(m^2 \cdot s \cdot^\circ C)$ for test 12) since the two tests have a different setting of the jet diameter D, which has been proved to be the most important parameter influencing the heat transfer

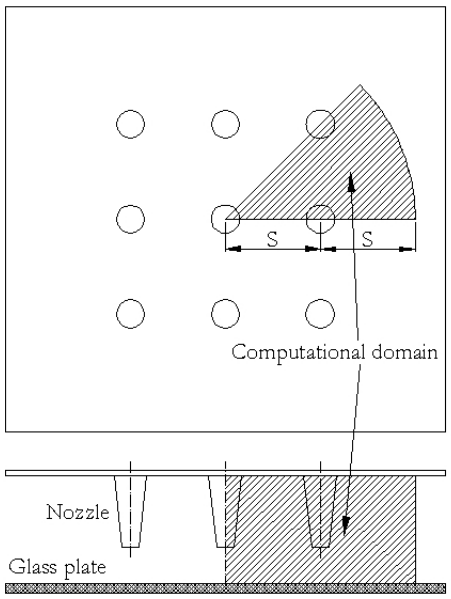

Fig. 4. Computational domain. The radius of the model is set to double the jet-to-jet distance. Considering the symmetrical behavior of the physical phenomenon only an octave of the entire volume has been built and meshed.

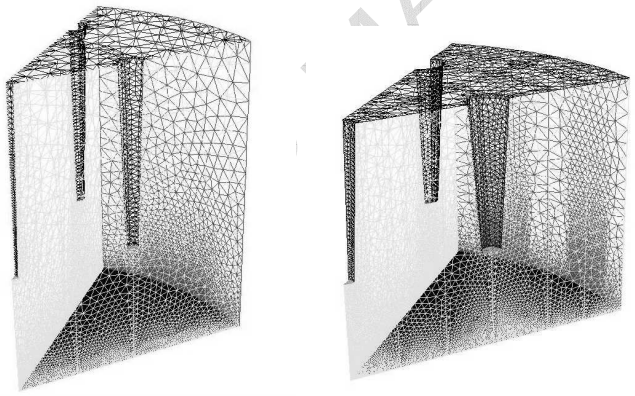

(a) Test2. (b) Test12.

Fig. 5. Model and mesh of tests 2 and 12 are shown as an example. The CFD software was left in charge of the model mesh generation, once the element dimensions are imposed.

coefficient during the cooling process. The local heat transfer coefficient was integrated over the glass plate area to determine the average heat transfer coefficient (h). The three maximum values occurring on the air jet impingement areas were then averaged ("Peak")and this value used to construct the "Uniformity Parameter" (U) which is given by:

$$Uniformity\ Parameter = \frac{Peak}{Aver.\ heat\ transfer\ coefficient}$$

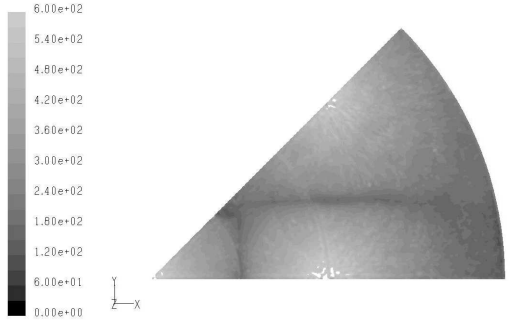

(a) Test2.

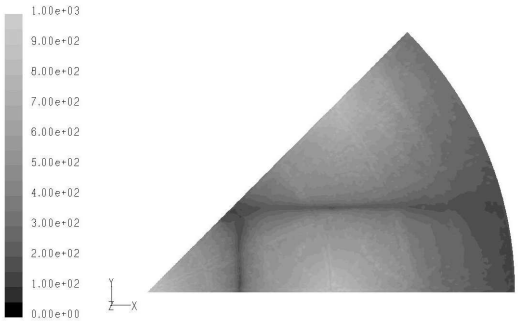

(b) Test12.

Fig. 6. Test results: local heat transfer coefficient on the glass plate for tests 2 and 12. A different scale for the h values has been used (600 $J/(m^2 \cdot s \cdot^\circ C)$ for test 2 and 1000 $J/(m^2 \cdot s \cdot^\circ C)$ for test 12) since the two tests have a different setting of the jet diameter D, which has been proved to be the most important parameter influencing the heat transfer coefficient during the cooling process.The local heat transfer coefficient was integrated over the glass plate area to determine the average heat transfer coefficient. The three maximum values, corresponding with the core jet impingement, are then averaged ("Peak") to construct the "Uniformity Parameter" used as a Target Function of the DOE analysis.

The higher the Uniformity Parameter, the higher the local heat transfer coefficient gradient on the glass plate, the lower the cooling uniformity. In Table 2 the output results (average heat transfer coefficient on the glass plate, Peak and Uniformity parameter) of the sixteen CFD simulations are shown. The effect of the control parameters (on h and U) and the overall mean values are shown in Table 3.

As already said, once the element dimensions are imposed, the software was left in charge of the model mesh generation. The element dimensions on the model surface - once an upper limit has been determined from a previous 2D analysis - can vary within a range of values depending on the model size. The larger the model (e.g. with $D = 8, S = 60$ and $Sp = 60$), the larger the element size that has been used - especially for surfaces that are not close to the glass plate - with the aim of limiting the computational effort. For the same reason, the sixteen models present different values of the mesh generation parameter used for the proper determination of the internal-to-surface

Table 2
Results of the sixteen CFD simulations: h (average heat transfer coefficient), Peak and U (Uniformity Parameter).

	Control Parameters					**Results**		
Test n.	D	H	S	Sp	V	h	Peak	U
1	4	40	40	20	110	262	564	2.15
2	4	40	40	60	140	312	617	1.98
3	4	40	60	20	140	237	610	2.57
4	4	40	60	60	110	211	517	2.45
5	4	60	40	20	140	292	533	1.83
6	4	60	40	60	110	255	477	1.87
7	4	60	60	20	110	195	415	2.13
8	4	60	60	60	140	237	527	2.22
9	8	40	40	20	140	516	918	1.78
10	8	40	40	60	110	430	747	1.74
11	8	40	60	20	110	331	678	2.05
12	8	40	60	60	140	421	867	2.06
13	8	60	40	20	110	369	708	1.92
14	8	60	40	60	140	498	890	1.79
15	8	60	60	20	140	391	870	2.23
16	8	60	60	60	110	328	712	2.17

ratio of the element dimensions. These differences, from model to model, in mesh size and structure, can cause an effect on the target function values (quality parameters) that can not be traced back to a control parameter effect. This mesh-effect (i.e. the result's uncertainty due to the model mesh) has been considered as a source of experimental error and evaluated using replications, where little variation on the elements dimensions and on mesh generation parameter have been applied (inside the range of allowable values above mentioned). Table 4 shows results of three replications of Test 1 and Test 13.
To evaluate the significance of each control parameter effect compared to the experimental error, the $F - ratio$ has been calculated. The $F - ratio$ of a control parameters is given by:

$$F = \frac{MS}{Se^2}$$

Table 3
Analysis of Means results.

(a) Control parameter effects.

				Effects	
	Level	av.h	av.U	h	U
D	4mm	250	2.15	160	-0.18
	8mm	410	1.97		
H	40mm	340	2.10	-19	-0.08
	60mm	321	2.02		
S	40mm	367	1.88	-73	0.35
	60mm	294	2.23		
Sp	20mm	324	2.08	12	-0.05
	60mm	336	2.03		
V	110m/s	298	2.06	65	0.00
	140m/s	363	2.06		

(b) Overall mean values.

Av.h	Av.U
330	2.06

Table 4
Results of three replications of Test1 and Test13.

		Replications				Replications		
	Test 1	1	2	3	**Test 13**	1	2	3
h	**262**	275	258	264	**369**	388	362	355
U	**2.15**	2.15	2.24	2.26	**1.92**	1.74	1.99	1.85

Where:
MS=Mean Square due to a control factor
Se^2=Mean Square due to experimental error. The mean square for a control factor is defined by

$$MS = \frac{factor\ effect\ Sum\ of\ Squares(SS)}{factor\ Degree\ Of\ Freedom(DOF_f)}$$

The sum of squares due to experimental error determined by replication can be calculated as follows:

$$Se^2 = \frac{1}{r-1}\sum_{j=1}^{n}(RR_j - \overline{RR})^2$$

Table 5
Calculation of the mean square due to experimental error for replications of Test1 and Test13.

	Test 1	RR_1	RR_2	RR_3	**Av.RR**	**Se^2**
h	**262**	275	258	264	**264.8**	**53**
U	**2.15**	2.15	2.24	2.26	**2.2**	**0.00328**

	Test 13	RR_1	RR_2	RR_3	**Av.RR**	**Se^2**
h	**369**	388	362	355	**368.5**	**202**
U	**1.92**	1.74	1.99	1.85	**1.87**	**0.01146**

Table 6
$F-ratio$ values of Control parameters effect on h and U. Sp is the only parameter that has a moderate effect on both the target functions. H and V have a moderate effect on U compared to experimental error.

	MS		**F-Ratio**	
	h	U	h	U
D	102,787	0.1400	509	12.2
H	1,513	0.0329	7	2.9
S	21,237	0.5013	105	44
Sp	614	0.0406	3	3.5
V	17,101	0.0291	85	2.5

where r is the number of replicated measurements, RR_j are the individual response values considered, and $\overline{RR}$ is the average of the replicate RR values. In our case the mean square due to a control factor equals the factor effect sum of squares since $DOF_f = 1$ for each control parameter.
A strong control parameter effect, compared to experimental error, occurs when $F \geq 4$. For $1 \leq F \leq 4$ the control parameter has only a moderate effect compared to experimental error and for $F < 1$ the control factor effect is indistinguishable from the experimental error(23).
Table 5 shows the Se^2 values calculated for test1 and test13 separately. Table 6 displays the MS and $F-ratio$ values for each control factor effect on the quality parameters h and U. Following a conservative approach, the highest Se^2 values (test13 for both h and U) has been considered in the $F-ratio$ calculation .
It can be seen that Sp is the only control parameter that has a moderate effect on both the target functions, while the effect of the other four parameter

on h outweighs the experimental error effect. H and V also have a moderate effect on U, compared to experimental error.
The same analysis was conducted on the columns of the orthogonal array containing interaction effect, to evaluate the significance of interference compared to experimental error.

Table 7 shows the two-way interaction effect on h and U and the calculated values of MS $(= SS)$ and $F-ratio$. Considering the average heat transfer coefficient value (h), the two-way interference effect DxH, DxS and SxV have a moderate significance while the interference effect of DxV is strong compared to experimental error. Considering now the uniformity parameter (U), the interference effect between D and H $(D$x$H)$ is clearly significant while SxV has a moderate effect compared to experimental error. All the other two-parameter interactions have a negligible effect on the target functions.
To quantitatively evaluate the control parameter interaction - necessary to create the mathematical model - the dependence between a control factor effect and the level assumed by a second control parameter has also been evaluated. Interactions that show a moderate or relevant effect $(F > 2)$ compared to experimental error have been plotted in fig.7. In particular fig.7(a) and 7(b) display the interaction effects of DxS $(F = 3.1)$ and DxV $(F = 13.8)$ on h, and in fig.7(c) the interaction effect of DxH $(F = 10.8)$ on the uniformity parameter value (U) is plotted. It is interesting to observe that the interactions DxS and DxV on h are both monotonic (or synergistic) while the DxH interaction on U is antisynergistic that is, the slope of a control parameter effect plots changes sign depending upon the second parameter's level.
A parametric prediction model has been created using the relationship between control parameter effects, interference and the calculated output results (i.e. target functions h and U). In particular, linear variable relationships have been considered between control parameters and target functions, the slope of which (of the linear relations) depends upon interaction between the control parameters. To simplify the analysis and the mathematical model, the control factor Sp has been left out of the predictive model since it is the only parameter that has a moderate effect on both the target functions. Sp also shows no relevant interaction with the other four parameters. Furthermore, only the interactions with an $F - ratio > 2$ have been implemented in the model.
Table 8 shows a comparison between the CFD simulations output values with those calculated using the predictive model (M). In fourth, fifth, eighth and ninth columns the absolute $(|e|)$ and percentage deviations $(e\% = \frac{|e|}{CFD\ result}100)$ are shown.

Note that the predictive model is not a discrete model. Thus, it allows calculation of the target functions also for a set of the control parameter values not corresponding to those considered within the sixteen simulations. However the model's validity is guaranteed if the control parameter values are chosen within the ranges defined by the factor levels.
Two further simulations (Valid01 and Valid02) have been performed taking

Table 7
Mean Square and $F-ratio$ values of interactions effect on h and U. Only the two-way interactions DxS and DxV have been implemented in the mathematical model for the prediction of the average heat transfer coefficient, since they have respectively a moderate and a relevant effect on h compared to experimental error. Similarly only the DxH interaction has been considered for the prediction of the Uniformity Parameter U.

				Effects		**SS=MS**		**F-Ratio**	
	Level	Av.h	Av.U	h	U	h	U	h	U
DxH	1	326	2.16	9	-0.20	298	0.1563	1.5	13.6
	2	335	1.96						
DxS	1	324	2.04	13	0.03	630	0.0045	3.1	0.4
	2	337	2.07						
HxS	1	334	2.05	-7	0.02	207	0.0013	1.0	0.1
	2	327	2.07						
SpxV	1	328	2.04	5	0.04	77	0.0071	0.4	0.6
	2	333	2.08						
DxSp	1	333	2.05	-5	0.01	108	0.0002	0.5	0.0
	2	328	2.06						
HxSp	1	333	2.08	-5	-0.04	119	0.0050	0.6	0.4
	2	328	2.04						
SxV	1	325	2.09	10	-0.07	411	0.0218	2.0	1.9
	2	335	2.02						
SxSp	1	329	2.07	2	-0.03	11	0.0033	0.1	0.3
	2	331	2.04						
HxV	1	332	2.06	-3	0.00	24	0.0001	0.1	0.0
	2	329	2.06						
DxV	1	344	2.06	-27	0.00	2,851	0.0000	14.1	0.0
	2	317	2.06						

into account values of the control parameters not corresponding to those defined by the factor levels. In Table 9 the test setting and results are shown. It can be seen the good correspondence between CFD and Model results also for these two simulations, whose control parameter settings has not been considered within the sixteen DOE simulations.

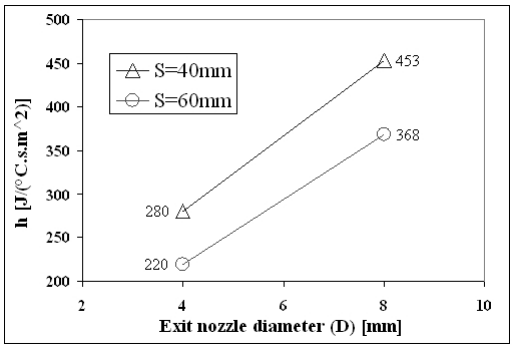

(a) DxS.

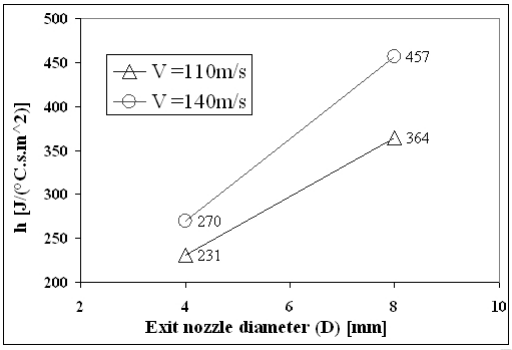

(b) DxV.

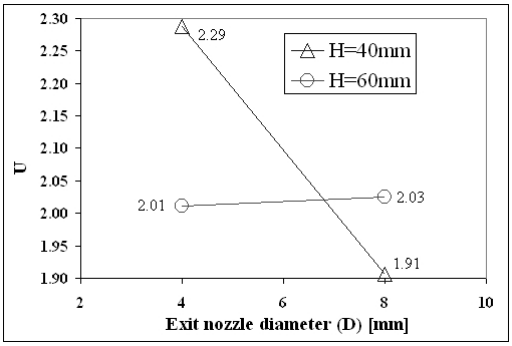

(c) DxH.

Fig. 7. Interaction plot of moderate and relevant parameter interference. The interactions DxS and DxV on h (fig.7(a), 7(b)) are both monotonic (or synergistic) while the DxH interaction on U (fig.7(c)) is antisynergistic. This means that the slope of a control parameter effect plots changes sign depending upon the second parameter's level.

4 Conclusions

The results of the present work have been succesfully applied in the design of an innovative reconfigurable blower. Implemented in a Visual Basic application - together with formulas that take into account the glass plate hardenability - the mathematical model found have speeded up the performance comparison of different blower configurations in the design stage without the necessity of performing further CFD simulations. Thus, this tool has great usefulness for technicians and engineers who are not accustomed to managing finite element codes.

Great economical savings of impeller costs are achievable by choosing a control parameter configuration that guarantees the requested average heat transfer coefficient and uniformity parameter values, with the minimum in spent air

Table 8
CFD simulations-predictive model (M) results comparison of h and U output values.

Test n.	h(CFD)	h(M)	|e(h)|	e(h)%	U(CFD)	U(M)	|e(U)|	e(U)%
1	262	260	2	0.9	2.15	2.06	0.09	4.4
2	312	324	12	3.8	1.98	1.94	0.04	1.9
3	237	243	6	2.5	2.57	2.49	0.08	3.3
4	211	204	7	3.3	2.45	2.45	0.00	0.1
5	292	298	6	2.1	1.83	1.88	0.05	2.7
6	255	253	2	0.8	1.87	1.86	0.01	0.4
7	195	180	15	7.7	2.13	2.33	0.21	9.6
8	237	240	3	1.3	2.22	2.26	0.04	1.8
9	516	500	16	3.1	1.78	1.82	0.04	2.2
10	430	430	0	0.0	1.74	1.77	0.04	2.2
11	331	338	7	2.1	2.05	2.1	0.05	2.4
12	421	422	1	0.2	2.06	2.06	0.00	0.1
13	369	383	14	3.9	1.92	1.87	0.05	2.6
14	498	487	11	2.2	1.79	1.79	0.01	0.4
15	391	391	0	0.00	2.23	2.16	0.07	3.0
16	328	333	5	1.5	2.17	2.12	0.05	2.4

mass and air velocity values (i.e. the impeller performance characteristics). It must be remembered that the impeller-blower costs could represent one half of the entire glass forming and tempering plant costs.

Combining Design Of Experiments tools and the finite element analysis provides an effective approach to optimize a mechanical system in the design stage. Furthermore, this approach is successful in identifying the design parameters that have the most influence on the quality characteristics of the systems (i.e. the target functions).

Table 9
To verify that the mathematical model performs correctly, two further CFD models have been created using values of the control parameters not corresponding to those defined by the factor levels. The test setting is shown in Table 9(a), while Table 9(b) displays the comparison with the predictive model output. The absolute and percentage deviations are congruent to those calculated for the sixteen simulations, shown in Table 8.

(a) Test setting.

	D	H	S	Sp	V
Valid 01	5	50	55	30	120
Valid 02	7	55	45	50	132

(b) CFD test results and comparison with mathematical model output.

Test n.	h(CFD)	h(M)	|e(h)|	e(h)%	U(CFD)	U(M)	|e(U)|	e(U)%
Valid 01	254	264	10	3.9	2.17	2.05	0.12	5.5
Valid 02	401	405	4	1.0	1.82	1.89	0.07	3.8

Acknowledgements

The present work was supported by Techint SpA - Business Unit: Glass Plants STM - of Calvenzano, Bergamo, Italy. The authors wish to thank Gerolamo Fasce, Ivan Bruneri and Vittorio Pagani for their contributions.

References

[1] Jung-Yang San, Mao-De Lai, Optimum jet-to-jet spacing of heat transfer for staggered arrays of impinging air jets, Int. J. Heat and Mass Transfer 44 (2001) 3997–4007.

[2] H. Martin, "Heat and mass transfer between impinging gas jets and solid surfaces", Adv. Heat Transfer, vol.13, pp. 1–60, 1977.

[3] Jung-Yang San, Chih-Hao Huang and Ming-Hong Shu, Impingement cooling of a confined circular air jet, Int. J. Heat and Mass Transfer 40 (6) (1997) 1355–1364.

[4] A.M. Huber, R. Viskanta, Convective heat transfer to a confined impinging array of air jets with spent air exits, J. Heat Transfer 116 (1994) 570–576.

[5] A.M. Huber, R. Viskanta, Effect of jet-jet spacing on convective heat transfer to confined impinging arrays of axisymmetric air jets, Int. J. Heat and Mass Transfer 37 (18) (1994) 2859–2869.

[6] A.M. Huber, R. Viskanta, Comparison of convective heat transfer to perimeter and center jets in a confined impinging array of axisymmetric air jets, Int J. Heat and Mass Transfer 37 (18) (1994) 3025–3030.

[7] Dong-Ho Rhee, Pil-Hyun Yoon, Hyung Hee Cho, Local heat/mass transfer and flow characteristics of array impinging jets with effusion holes ejecting spent air, Int J. Heat and Mass Transfer 46 (2003) 1049–1061.

[8] Jung-Yang San, Wen-Zheng Shiao, Effect of jet plate size and plate spacing on the stagnation Nusselt number for a confined circular air jet impinging on a flat surface, Int J. Heat and Mass Transfer 49 (2006) 3477–3486.

[9] E. Baydar, Y. Ozmen, An experimental and numerical investigation on a confined impinging air jet at high Reynolds numbers, Applied Thermal Engineering 25 (2005) 409–421.

[10] D.W. Colucci, R. Viskanta, Effect of nozzle geometry on local convective heat transfer to a confined impinging air jet, Experimental Thermal and Fluid Science 13 (1996) 71–80.

[11] Bertrand P.E. Dano, James A. Liburdy, Koonlaya Kanokjaruvijit, Flow characteristics and heat transfer performances of a semi-confined impinging array of jets: effect of nozzle geometry, Int. J. Heat and Mass Transfer 48 (2005) 691–701.

[12] X. Yan, N. Saniei, Heat transfer from an obliquely impinging circular air jet to a flat plate, Int. J. Heat and Fluid Flow 18 (1997) 591–599.

[13] R. Gardon, J. Cobonpue, Heat transfer between a flat plate and jets of air impinging on it, Int Developments in Heat Transfer, Proceedings of the 2nd Int. Heat Transfer Conference, American Society of Mechanical Engineers, New York, 1962.

[14] R. Gardon, The tempering of flat glass by forced convection, VII Int. Cong. On Glass, Paper 79, London, 1965.

[15] R. Gardon, J.C. Akrifat, Heat transfer characteristics of impinging two-dimensional air jets, J. Heat Transfer 88 (1966) 101–108.

[16] Matt Goodro, Jongmyung Park, Phil Ligrani, Mike Fox, Hee-Koo Moon, Effects of Mach number and Reynolds number on jet array impingement heat transfer, Int. J. Heat and Mass Transfer 50 (2007) 367–380.

[17] D.C. Montgomery, Design and Analysis of Experiments, J.Wiley and Sons, 3rd edition, 1991.

[18] C.F. Jeff Wu, Michael Hamada, Experiments: Planning, Analysis and Parameter Design Optimization, Wiley Interscience, 1st edition, 2000.

[19] Chang-Xue Jack Feng, Anthony L.Saal, James G. Salsbury, Arnold R. Ness, Gary C.S. Lin, Design and analysis of experiments in CMM measurement uncertainty study, Precision Engineering 31 (2007) 94-101.

[20] F.M. Shuaeib, A.M.S. Hamouda, S.V. Wong, R.S. Radin Umar, M.M.H. Megat Ahmed, A new motorcycle helmet liner material: The finite element simulation and design of experiment optimization, Materials and Design 28 (2007) 182-195.

[21] S.K. Roy, R. Dey, A. Mitra, S. Mukherjee, M.K. Mitra, G.C. Das, Optimization of process parameter for the synthesis of silica gel-WC nanocom-

posite by design of experiment, Materials Science and Engineering C 27 (2007) 725-728.

[22] G. Taguchi, S. Konishi, Taguchi methods ortoghonal arrays and linear graphs, American Supplier Inst, 1987.

[23] W.Y. Fowlkes , C. M. Creveling, Engineering Methods for Robust Product Design, Addison Wesley, 2000.